RASĀYAN *J. Chem.*
Vol. 19 | No. 2 | 1150-1157| April-June | 2026
ISSN: 0974-1496 | e-ISSN: 0976-0083 | CODEN: RJCABP
http://www.rasayanjournal.com
http://www.rasayanjournal.co.in

ENHANCED DSSC EFFICIENCY THROUGH Sb-DOPED ZnO THIN FILMS SYNTHESIZED VIA SOL-GEL SPIN COATING WITH PURPLE SWEET POTATO ANTHOCYANIN SENSITIZER: EFFECT OF DOPING CONCENTRATION AND ANNEALING TEMPERATURE ON PHOTOVOLTAIC PERFORMANCE

Motlan✉, K. Sinulingga, and N. Siregar
Department of Physics, Faculty of Mathematics and Natural Sciences, Universitas Negeri Medan, Medan, North Sumatra, Indonesia
✉Corresponding author: motlan@unimed.ac.id

ABSTRACT
The global transition toward sustainable energy demands low-cost, eco-friendly photovoltaic technologies accessible to developing economies. This work addresses this challenge by preparing and characterizing Sb-doped ZnO thin films via sol-gel spin coating, evaluated as photoanodes in Dye-Sensitized Solar Cells (DSSCs) sensitised with purple sweet potato (Ipomoea batatas) anthocyanin, directly supporting SDG 7 (Affordable and Clean Energy). Films containing 2.0 to 4.0 wt% Sb were deposited on FTO substrates and annealed between 400 and 600°C. XRD confirmed a hexagonal wurtzite crystal structure with grain dimensions growing from 17.76 nm at 400°C to 28.39 nm at 600°C. SEM revealed well-formed hexagonal nanoparticle surfaces, and EDS validated successful Sb integration. UV-Vis analysis showed a thermally adjustable bandgap spanning 3.35 to 3.41 eV, with peak optical properties at 550°C. Photovoltaic testing demonstrated that 3.5 wt% Sb achieved the highest power conversion efficiency of 0.453% (Voc = 0.64 V, Jsc = 1.20 mA/cm², FF = 59.0%), representing a 43% improvement over the 2.0 wt% Sb reference (0.316%). These findings establish clear composition-structure-performance relationships for Sb-doped ZnO photoanodes with natural sensitizers, providing a foundational framework for future advances in sustainable, low-cost solar cell development for energy-scarce communities
Keywords: ZnO, Spin Coating, Purple Sweet Potato, Photovoltaic
RASĀYAN *J. Chem.*, Vol. 19, No.2, 2026

INTRODUCTION

The intensification of climate change, rapid exhaustion of fossil fuel reserves, and surging energy consumption driven by industrial expansion, transportation networks, and demographic growth have made it imperative to accelerate advances in renewable energy technologies.[1] Among the many clean energy alternatives available, including wind power, biomass conversion, and hydroelectric generation[2], photovoltaic solar energy has attracted considerable and growing interest from both the scientific community and the industrial sector.[3] Mainstream photovoltaic devices today predominantly rely on silicon-based semiconductor materials[4], binary compound semiconductors exemplified by cadmium telluride (CdTe)[5], as well as organic semiconductor materials such as polyphenylene vinylene derivatives and fullerene compounds.[6] Nonetheless, metal oxide semiconductors such as zinc oxide (ZnO) and its doped variants represent attractive candidates for broadening the material landscape in photovoltaic device construction. Nanostructured ZnO has proven particularly valuable in serving as photoanode materials within Dye-Sensitised Solar Cells (DSSCs), where it facilitates charge transport at interfaces and contributes to improved power conversion efficiency (PCE). ZnO is distinguished by a direct and wide bandgap of 3.37 eV[7] together with an exciton binding energy of 60 meV, and it possesses favorable optical, electrical, and piezoelectric attributes that make it suitable for optoelectronic applications.[8] Despite these favourable characteristics, DSSC efficiencies remain insufficient for widespread commercial deployment, necessitating ongoing refinement of ZnO fabrication quality, preparation methodologies, and sensitiser selection. Various deposition techniques have been explored, including

molecular beam epitaxy (MBE), metal-organic chemical vapour deposition (MOCVD), radio-frequency sputtering, spray pyrolysis, and pulsed laser deposition, each carrying practical drawbacks such as high equipment costs and complex safety protocols. In contrast, sol-gel spin coating[9] alongside electrochemical deposition techniques[10] have gained traction as more affordable and accessible routes for producing ZnO thin films. The incorporation of metallic dopants into ZnO has been widely studied to boost DSSC performance metrics. Published work has reported conversion efficiencies as high as 3.53% when using Mg-doped ZnO[11], 2.03% for copper-doped ZnO[12], and a range of values for lithium-doped ZnO[13], all pointing to significant opportunities for further performance gains. Prior work on antimony (Sb)-doped ZnO has shown enhanced absorbance and transmittance at Sb loadings near 3%. Accordingly, fine-tuning the structural, morphological, optical, and electrical attributes of ZnO through deliberate Sb doping is a key strategy for advancing DSSC efficiency. The choice of a suitable dye sensitizer that is chemically compatible with the Sb-doped ZnO surface is equally important, since the physicochemical match between the oxide and dye governs sensitization quality. Researchers have investigated a variety of plant-based natural dyes as sensitizers[14], though none has achieved optimal results, largely because of acidity mismatch with the oxide surface. Purple sweet potato anthocyanin emerges as a particularly promising candidate, offering improved acid-base compatibility with Sb-doped ZnO surfaces while preserving adequate absorption of visible light. Although research on Sb-doped ZnO as DSSC photoanodes is growing, the interplay between Sb concentration and annealing temperature on device performance with natural anthocyanin sensitizers remains underexplored. This gap motivates the present work, which seeks to map clear composition-structure–property–performance linkages in this material system. The research also aligns with Sustainable Development Goal 7 (SDG 7: Affordable and Clean Energy) by focusing on low-cost devices built from earth-abundant oxide materials and plant-based sensitizers. Specifically, Sb-doped ZnO thin films were synthesized by sol-gel spin coating for use as DSSC working electrodes sensitized with purple sweet potato dye, and the effects of Sb concentrations (2%, 2.5%, 3%, 3.5%, and 4%) and annealing temperatures (400, 500, 550, and 600°C) on film properties and device efficiency were systematically examined.

EXPERIMENTAL

Materials and Methods

Zinc acetate dihydrate [$Zn(CH_3COO)_2 \cdot 2H_2O$], antimony (Sb), isopropanol (C_3H_8O), and diethanolamine (DEA, $C_4H_{11}NO_2$) from MERCK Germany were used as precursor, dopant, solvent, and stabilizer, respectively. Sb-doped ZnO thin films with concentrations of 2.0, 2.5, 3.0, 3.5, and 4.0 wt% were deposited on fluorine-doped tin oxide (FTO) glass substrates via the sol-gel spin coating method. Zinc acetate dihydrate was doped with varying Sb concentrations and dissolved in isopropanol under magnetic stirring, followed by the addition of DEA until a clear, transparent solution formed. The sol-gel was deposited dropwise onto FTO substrates and spun at 5000 rpm, then subjected to two-step thermal treatment: pre-heating at 200°C for 10 minutes and post-heating at temperatures ranging from 400 to 600°C for 5 hours. For DSSC fabrication, the Sb-doped ZnO thin films were immersed in natural dye extracted from purple sweet potato (*Ipomoea batatas*) for sensitisation. The dye-sensitised photoanode and platinum counter electrode were assembled using Surlyn polymer as a separator, sealed by heating at 70-80°C, and the electrolyte solution was injected through a small hole to complete the device. X-ray diffraction (XRD) with Cu Kα radiation (λ = 1.5418 Å) was employed to analyze crystallographic phases. Scanning electron microscopy (SEM) coupled with energy dispersive X-ray spectroscopy (EDS) characterized surface morphology and elemental composition. UV-Vis spectrophotometry measured absorbance and transmittance spectra (300-700 nm), with optical band gap energy determined via the Tauc plot method. Photovoltaic performance was evaluated through current density-voltage (J-V) curves using a digital multimeter and solar simulator.

RESULTS AND DISCUSSION

Temperature-Dependent Structural Evolution and Thermal Processing Optimisation

XRD patterns from ZnO: Sb films annealed between 400°C and 600°C (Fig.-1) confirmed that the hexagonal wurtzite structure was preserved at all temperatures, with the principal reflections at (100), (002), and (101) planes consistently yielding a c/a ratio of 1.602.[15,16]

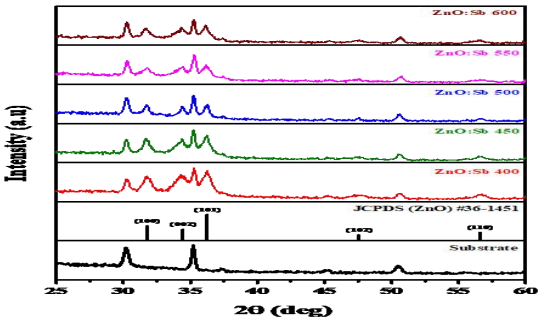

Fig.-1: X-ray Diffraction Spectra of ZnO: Sb, Heating Temperature Variation

Table-1 documents pronounced grain coarsening, with crystallite dimensions enlarging from 17.76 nm at 400°C to 28.39 nm at 600°C, approximately a 60% increase, driven by thermally activated grain boundary migration and atomic redistribution.[17,18]

Table-1: Crystal size of ZnO: Sb Thin Film, Variation of Heating Temperature

Samples	Crystal Size (nm)
ZnO: Sb 400	17.76
ZnO: Sb 450	21.80
ZnO: Sb 500	26.66
ZnO: Sb 550	25.40
ZnO: Sb 600	28.39

Crystallite growth did not follow a simple monotonic trend; the largest dimensions (28.39 nm) appeared at 600°C, while 550°C produced slightly smaller values (25.40 nm). This behavior points to competing processes, including grain coalescence and secondary nucleation or stress-driven refinement operative within specific temperature ranges.[19] The consistent narrowing of XRD diffraction peaks with rising annealing temperature further confirms an ordered improvement in crystallographic quality and a corresponding reduction in internal lattice strain.[20]

Compositional Stability and Morphological Transformations

SEM imaging revealed how film morphology evolved with annealing temperature (Fig.-2). Films treated at 400°C showed a fine-grained, porous surface typical of incompletely densified sol-gel coatings. Progressive temperature elevation drove morphological maturation: samples annealed at 450 to 500°C showed improved inter-grain contact and bridging between adjacent crystals, while those treated at 550 to 600°C developed compact, faceted surfaces bearing well-formed hexagonal grain shapes characteristic of thermodynamically stabilised crystal growth.[21]

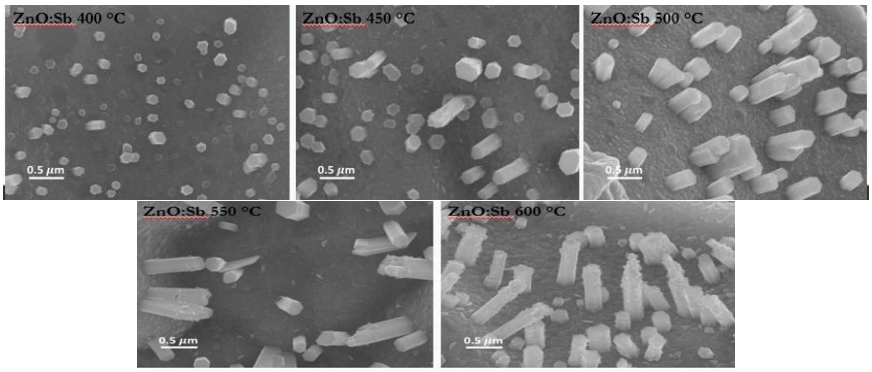

Fig.-2: SEM Photos of the Surface of ZnO: Sb Thin Films with Variations in Heating Temperature: a. 400°C, b. 450°C, c. 500°C, d. 550°C and e. 600°C

EDS analysis (Fig.-3, Table-2) highlighted temperature-dependent Sb retention trends. Peak Sb content (2.31 at%) was measured at the lowest annealing temperature of 400°C, after which concentrations

declined and fluctuated between 1.54 and 2.27 at% at elevated temperatures.[22] Interestingly, Sb content at 600°C (2.27 at%) nearly matched that at 400°C, suggesting lattice redistribution or reintegration of Sb at extreme temperatures. This irregular trend reflects complex competing kinetics involving Sb_2O_3 volatilisation and elemental sublimation on one hand, and solid-state lattice diffusion and grain boundary trapping on the other.[23]

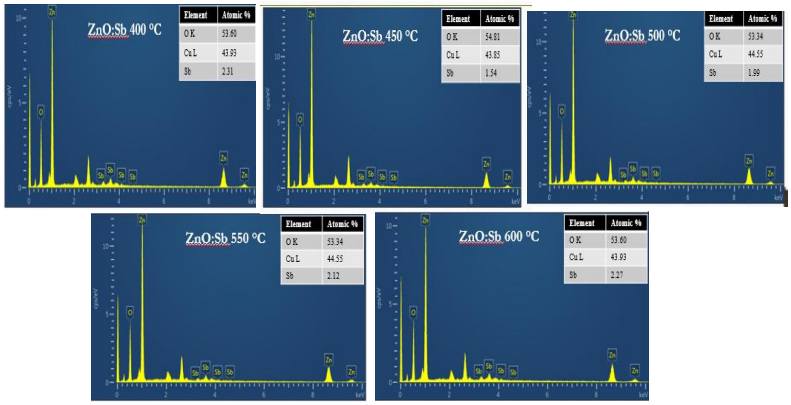

Fig.-3: EDS Spectrum of ZnO: Sb Thin Films with Varying Antimony Doping

The consistently oxygen-rich stoichiometry (O: Zn exceeding 1.0) together with a Zn deficit observed under all annealing conditions confirms that intrinsic defects, particularly interstitial oxygen and zinc vacancies, are the primary drivers of n-type conductivity in these films, independent of the extrinsic Sb dopant level.[24] This inherent compositional trait is beneficial for photovoltaic operation, since an elevated electron carrier density promotes more efficient charge extraction and transport.

Table-2: Atomic Percentage of ZnO: Sb Heating Temperature Variation

Sampel (°C)	Sb (%)	Zn (%)	O (%)
ZnO: Sb (400)	2.31	43.93	53.60
ZnO: Sb (450)	1.54	43.85	54.81
ZnO: Sb (500)	1.99	44.55	53.34
ZnO: Sb (600)	2.27	43.93	53.60

Thermal Engineering of Optical Response

UV-Vis measurements performed on thermally treated films (Fig.-4) revealed a systematic evolution of optical properties that is distinct from purely composition-driven changes. With increasing annealing temperature, absorption intensities in the ultraviolet region (320 to 370 nm) progressively increased while spectra became more defined, an outcome attributed to a thermally driven reduction in defect density and a corresponding improvement in the electronic band structure.[25] Transmittance data indicated that the highest average visible transparency (approximately 85%) was achieved at intermediate annealing temperatures, with 550°C offering the best balance between crystalline quality and surface smoothness.

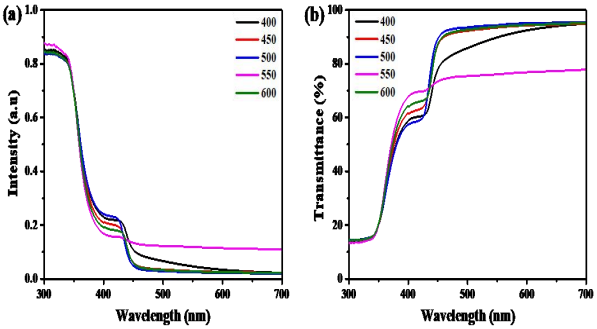

Fig.-4: (a) Absorbance Spectrum of Heating Temperature Variation, and (b) Transmittance Spectrum of Heating Temperature Variation

Tauc plot analysis of UV-Vis absorption data (Fig.-5) revealed that thermal processing enabled bandgap adjustment over a range of 3.35 to 3.41 eV. The narrowest bandgap (3.35 eV) was associated with 500°C treatment, related to incomplete crystallisation and a high density of mid-gap defect states. Annealing at 550°C yielded the widest bandgap (3.41 eV) through the combined effects of defect annihilation, favorable crystallite dimensions minimising grain boundary scattering, and a well-balanced Sb content supporting appropriate charge carrier levels.[26]

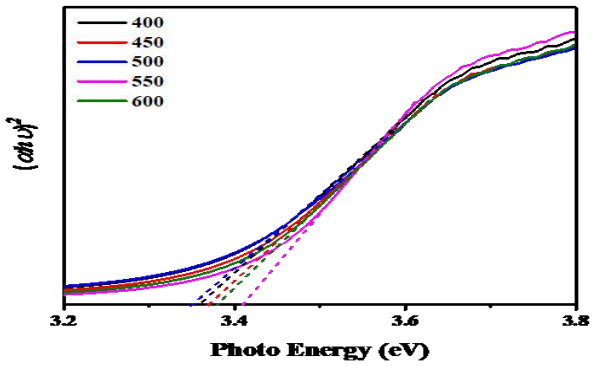

Fig.-5: Energy Band Gap Curve of ZnO:Sb Thin Films with Temperature Variation

Despite further grain growth, increasing the temperature to 600°C caused a slight bandgap narrowing to 3.37 eV, likely due to Sb volatilization-induced compositional shifts or thermally generated structural imperfections (Table-3).

Table-3: Energy Band Gap of ZnO:Sb, Heating Temperature Variation

Sample	Bandgap (eV)
ZnO: Sb (400)	3.36
ZnO: Sb (450)	3.37
ZnO: Sb (500)	3.35
ZnO: Sb (550)	3.41
ZnO: Sb (600)	3.37

These findings collectively identify 550°C as the optimal annealing condition, at which crystalline order, transmittance, bandgap magnitude, and dopant retention are concurrently maximized to provide the best photoanode performance.

Structure-Performance Relationships in Complete DSSC Devices

Measurements conducted on fully assembled DSSC devices using thermally optimized ZnO: Sb photoanodes at different Sb concentrations allowed direct composition-to-performance correlations to be drawn. Analysis of current density-voltage data (Fig.-6, Table-4) showed a clear compositional dependence of device parameters, with short-circuit current density (J*sc*) rising from 0.92 mA/cm² at 2.0% Sb to a peak of 1.20 mA/cm² at 3.5% Sb, then decreasing to 1.17 mA/cm² at 4.0% Sb.

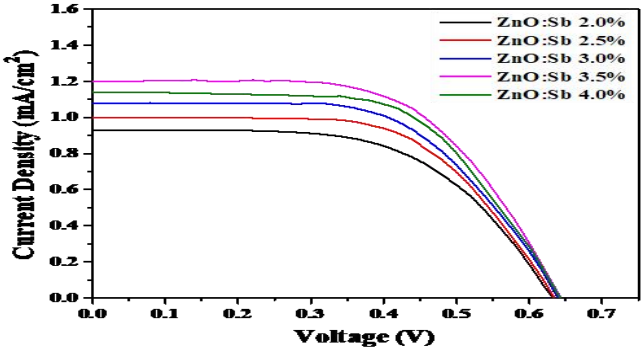

Fig.-6: Electrical Conductivity (J-V) Test Curve of ZnO: Sb Thin Film DSSC, Variation of Sb Doping

This bell-shaped dependence reflects the classical trade-off between increased carrier density, improving conductivity, and intensified ionised impurity scattering degrading carrier mobility in doped semiconductor materials.

The 30% improvement in J*sc* from 2.0% to 3.5% Sb corresponds to a power conversion efficiency increase from 0.316% to 0.453%, a relative improvement of 43% that demonstrates the strong impact of compositional optimisation. Open-circuit voltage remained constant at 0.64 V throughout the entire doping series, indicating that Sb incorporation in the 2 to 4 at% range does not appreciably shift the ZnO conduction band edge or disrupt the photoanode-electrolyte energetics. Fill factor improved progressively from 0.538 at 2% Sb to 0.590 at 3.5% Sb, reflecting reduced series resistance as photoanode conductivity increased with doping level. The minor efficiency decline at 4% Sb, despite higher carrier concentrations, suggests the emergence of limiting mechanisms such as increased defect-assisted recombination or reduced sensitizer uptake linked to morphological changes at excessive doping.

Table-4: Efficiency Parameters of ZnO:Sb Thin Films with Varying Sb Doping

Sampel	Voc (V)	Jsc (mA/cm²)	Pmax (W/cm²)	η (%)
ZnO: Sb 2.0%	0.64	0.92	53.8	0.316
ZnO: Sb 2.5%	0.64	0.99	56.9	0.361
ZnO: Sb 3.0%	0.64	1.08	58.4	0.404
ZnO: Sb 3.5%	0.64	1.20	59.0	0.453
ZnO: Sb 4.0%	0.64	1.17	56.9	0.426

Evaluated in the context of published efficiencies for metal-doped ZnO photoanodes, including Mg-doped systems at 3.53%[11], Cu-doped systems reaching 2.03%[12], and Li-doped variants with varying reported values[13] the present Sb-doped system demonstrates competitive performance, particularly considering natural dye utilisation. The modest absolute efficiency (<0.5%) reflects fundamental limitations of anthocyanin sensitisers: narrower absorption spectra, lower extinction coefficients, and reduced photostability compared to engineered ruthenium-based dyes achieving >11% efficiency. However, the systematic optimization methodology and clear identification of processing-performance relationships provide valuable foundational knowledge for continued development. From the perspective of SDG 7 (Affordable and Clean Energy), the present work demonstrates a technically viable and economically accessible approach to solar energy harvesting. The use of sol-gel spin coating with a low-cost, scalable deposition method. It is combined with an earth-abundant ZnO host and a plant-derived natural sensitiser, which minimizes the reliance on expensive or scarce materials. The 43% efficiency improvement achieved through simple compositional optimisation (3.5 wt% Sb) without any complex device architecture underscores the translational potential of this approach for decentralised energy generation in resource-limited settings, directly contributing to the goal of expanding access to affordable and clean energy.

CONCLUSION

This work successfully established a sol-gel spin coating route for preparing Sb-doped ZnO thin films and validated their function as photoanodes in anthocyanin-sensitised DSSCs, demonstrating a low-cost and eco-friendly approach in direct support of SDG-7 (Affordable and Clean Energy). Thermal treatment studies revealed that 550°C annealing produces the widest bandgap (3.41 eV) and optimal crystalline quality while preserving adequate dopant content, with grain sizes expanding from 17.76 nm at 400°C to 28.39 nm at 600°C. Among all compositions studied, 3.5 wt% Sb emerged as the optimal doping level, delivering a power conversion efficiency of 0.453%, a short-circuit current density of 1.20 mA/cm², an open-circuit voltage of 0.64 V, and a fill factor of 59.0%. This represents a 43% efficiency gain over the 2.0% Sb reference (0.316%), attributable to enhanced electrical conductivity, effective charge extraction, and a well-developed hexagonal nanocrystalline morphology favourable for dye uptake. The combination of optimized Sb-doped ZnO photoanodes with purple sweet potato anthocyanin sensitisers demonstrates a viable, affordable, and environmentally sustainable photovoltaic pathway. To further advance this system toward commercial relevance, future work should focus on: (i) engineering anthocyanin co-sensitisation with complementary dyes to broaden spectral absorption; (ii) optimising the ZnO-dye interface through surface passivation treatments; (iii) improving device encapsulation for long-term stability; and (iv)

scaling up fabrication using roll-to-roll sol-gel processes. These advances will help bridge the efficiency gap with conventional ruthenium-based DSSCs while maintaining the sustainability and affordability advantages central to SDG-7.

ACKNOWLEDGMENTS

This work was supported by the Institute for Research and Community Service of Universitas Negeri Medan, which has provided funding from the 2025 PNBP with contract number 0194/UN33/KPT/2025.

CONFLICT OF INTERESTS

The authors declare that there are no conflicts of interest.

AUTHOR CONTRIBUTIONS

The present work is related to *SDG-7: Affordable and Clean Energy*. All the authors contributed significantly to this manuscript, participated in reviewing/editing and approved the final draft for publication. The research profile of the authors can be verified from their ORCID ids, given below:

Motlan http://orcid.org/0000-0002-6246-0032
K. Sinulingga https://orcid.org/0000-0001-9758-7589
Nurdin Siregar http://orcid.org/0000-0001-8227-5582

Cite this article as: Motlan *et al.*, *Rasayan J. Chem.*, 19(2), 1150-1157(2026), https://doi.org/10.31788/RJC.2026.1929644.

REFERENCES

1. W. Cheng, L. Dan, X. Deng, J. Feng, Y. Wang, J. Peng, J. Tian, W. Qi, Z. Liu, X. Zheng, D. Zhou, S. Jiang, H. Zhao, X. Wang, *Scientific Data*, **9**, 83(2022), https://doi.org/10.1038/s41597-022-01196-7
2. T.M.N. Vo, C.N. Wang, F.C. Yang and V.T.T. Nguyen, *Eurasia Proceedings of Science, Technology, Engineering and Mathematics*, **26**, 356 (2023), https://doi.org/10.55549/epstem.1374936
3. S. Shukrullah, M.Y. Naz, K. Ali and S.K. Sharma, in Solar Cells: From Materials to Device Technology, Springer, Cham, pp. 139-164 (2020), https://doi.org/10.1007/978-3-030-36354-3_7
4. R. Parasuraman and K. Rathnakannan, *Journal of Computational Electronics*, **20**, 1851(2021), https://doi.org/10.1007/s10825-021-01769-6
5. K. Mykhailo, Z. Roman, K. Gennadiy, M. Kseniia, T. Roman and P. Dmytro, in Proceedings of the International Conference on Advanced Optoelectronics and Lasers (CAOL), Sozopol, Bulgaria, pp. 493-496 (2019), https://doi.org/10.1109/CAOL46282.2019.9019415
6. C.L. Gettinger, A.J. Heeger, J.M. Drake and D.J. Pine, *The Journal of Chemical Physics*, **101**, 1673(1994), https://doi.org/10.1063/1.468438
7. W. Amananti, R. Ardiyanto, H. Sutanto, I. Nurhasanah and I. Tivani, *Journal of Natural Sciences and Mathematics Research*, **8**, 43(2022), https://doi.org/10.21580/jnsmr.2022.8.1.9623
8. R. Sha, A. Basak, P.C. Maity and S. Badhulika, *Sensors and Actuators Reports*, **4**, 100098(2022), https://doi.org/10.1016/j.snr.2022.100098
9. Motlan and N. Siregar, *Journal of Physical Science*, **32**, 57(2021), https://doi.org/10.21315/JPS2021.32.1.5
10. N. Siregar, Motlan and M. Sirait, *Evergreen*, **10**, 432(2023), https://doi.org/10.5109/6792820
11. N. Siregar, Motlan, J.H. Panggabean, M. Sirait, J. Rajagukguk, N.S. Gultom and F.K. Sabir, *International Journal of Photoenergy*, **2021**, 4033692(2021), https://doi.org/10.1155/2021/4033692
12. H. Esgin, Y. Caglar and M. Caglar, *Journal of Alloys and Compounds*, **890**, 161848(2022), https://doi.org/10.1016/j.jallcom.2021.161848
13. S. Aksoy, O. Polat, K. Gorgun, Y. Caglar and M. Caglar, *Physica E: Low-Dimensional Systems and Nanostructures*, **124**, 114127(2020), https://doi.org/10.1016/j.physe.2020.114127
14. N. Siregar, Motlan and J.H. Pangabean, *Journal of Physical Science*, **32**, 69(2021),

https://doi.org/10.21315/jps2021.32.2.5
15. K.S. Babu, C.V. Reddy, Y. Suh and S.H. Park, *Rasayan Journal of Chemistry*, **12(1)**, 82(2019), https://doi.org/10.31788/RJC.2019.1215012
16. S. Kumar, S. Tiwari, S. Srivastava, V.K. Singh and R. Prakash, *Rasayan Journal of Chemistry*, **13(4)**, 2156 (2020), https://doi.org/10.31788/RJC.2020.1345823
17. R.M. German, P. Suri and S.J. Park, *Journal of Materials Science*, **44**, 1(2009), https://doi.org/10.1007/s10853-008-3008-0
18. K.R. Rajesh, A. Ramasamy, A. Pandikumar and K. Kannan, *Materials Today: Proceedings*, **23**, 144(2020), https://doi.org/10.1016/j.matpr.2019.06.659
19. G.K. Williamson and W.H. Hall, *Acta Metallurgica*, **1**, 22(1953), https://doi.org/10.1016/0001-6160(53)90006-6
20. J.Y.W. Seto, *Journal of Applied Physics*, **46**, 5247(1975), https://doi.org/10.1063/1.321593
21. Y. Zhao, C. Li, M. Chen, X. Yu, Y. Chang, A. Chen, H. Zhu and Z. Tang, *Materials Letters*, **251**, 178(2019), https://doi.org/10.1016/j.matlet.2019.05.065
22. Y. Caglar, M. Caglar and S. Ilican, *Journal of Materials Science: Materials in Electronics*, **30**, 2274(2019), https://doi.org/10.1007/s10854-018-0499-1
23. A. Khanna and V.K. Khanna, *Journal of Materials Science & Technology*, **35**, 1391(2019), https://doi.org/10.1016/j.jmst.2019.03.013
24. P. Sharma, S. Kumar and M. Singh, *Journal of Sol-Gel Science and Technology*, **113**, 1(2025), https://doi.org/10.1007/s10971-024-06545-0
25. T. Jiang, Y. Bu, X. Zhang, S. Qiao, H. Wang and T. Li, *Journal of Materials Chemistry C*, **8**, 14603(2020), https://doi.org/10.1039/D0TC03287E
26. M.Y.A. Rahman, A.A. Umar and M.M. Salleh, *Journal of Materials Science: Materials in Electronics*, **27**, 4722(2016), https://doi.org/10.1007/s10854-016-4351-0

[RJC-9644/2026]